The effect of microstructure on recrystallization and neutron irradiation defects annealing on two ITER specification tungsten

D. Papadakis[1,2] and K. Mergia[1,*]

[1] *Institute of Nuclear and Radiological Sciences and Technology, Energy and Safety, NCSR Demokritos, Athens, 15310, Greece*
[2] *Department of Physics, School of Sciences, University of Athens, Athens, 15772, Greece*

Abstract

The study of the recrystallization resistance of engineering grade tungsten (W) prior to and after neutron irradiation as well as subsequent thermal annealing provides valuable insight into neutron induced defect interactions and their kinetics as well as their correlation with recrystallization mechanisms. The outcome of such investigations would be of assistance for appropriate grade selection for a fusion reactor and the design of healing processes enabling the lifetime extension of fusion reactor components. Within this framework, samples from ITER specification W, forged bar and cold-rolled plate, were neutron irradiated to a dose of 0.18 dpa at 600 °C in the Material Test Reactor BR2, Mol, Belgium, and subsequently isochronally annealed from 700 to 1550 °C for 24 h with a 50 °C step with two non–irradiated counterparts. X-ray diffraction, optical microscopy and positron annihilation lifetime spectroscopy, combined with Vickers Hardness are used to correlate the recrystallization process and recovery mechanisms. It is found that the non-irradiated plate has a higher recrystallization resistance compared to that of the bar, with the former requiring 100 °C higher temperature for 24 h annealing time to recrystallize. Despite the irradiation induced dislocation loops and voids being of similar sizes and densities for both grades, the different initial microstructure affects the recrystallization process upon annealing, delaying it by 50 °C on the plate. Further in the plate a complete void dissolution is observed before recrystallization, which is not the case for the bar, for which the two effects occur at the same temperature.

Keywords: Tungsten, Post-Irradiation annealing, Recrystallization, X-ray diffraction, Vickers Hardness, Positron Annihilation Lifetime Spectroscopy

* **Corresponding author.** kmergia@ipta.demokritos.gr

1 Introduction

Tungsten (W) has been selected as the prime candidate material for plasma facing components (PFCs) of current and future fusion devices. This is due to its many superior properties, including high thermal conductivity, high melting point, low tritium retention, low swelling under irradiation, low sputtering yield, as well as resistance to thermal stress and shock [1–6]. The main drawbacks limiting its exploitation under service are its low ductile-to-brittle transition temperature (DBTT), fracture toughness and recrystallization temperature compared to the temperatures expected in a fusion environment. To cope with these issues, microstructural modifications have been proposed, with cold-rolling [7,8] and forging [9] producing ITER specification W [3,9,10] to be used as a reference to other material options.

In a future fusion reactor, high neutron fluxes originating from the D-T nuclear reaction will occur. The neutrons impinging on the materials cause displacement damage and transmutations. The displacement damage results in the creation of point defects which may aggregate to form vacancy clusters or voids and dislocation loops [11–16]. Neutron capture reactions can also occur, with rhenium (Re), osmium (Os) and tantalum (Ta) being the main transmutation products in tungsten [17] which can form precipitates [18] or clusters [19]. The specific type and population of defects are dependent on the neutron irradiation conditions [18,20–25].The fusion neutron irradiation damage is mimicked through the use of fission neutron irradiation [11,13,15–17,19–25] or ion irradiation [26–30].

Plasma facing components also have to withstand high heat fluxes accompanied by transient events such as edge-localized-modes (ELMs) and disruptions in the reactor, causing temperature increase and high thermal stresses in PFCs. This can lead to grain growth and recrystallization of W, and will eventually restore the W intrinsic brittleness by changing its deformed microstructure to a defect-free new grain structure. Consequently, the ability of the material to handle high thermal loads will be reduced and its lifetime will be limited. Therefore, it is of high importance to study the microstructural evolution of ITER grade tungsten after annealing in order to investigate the recovery stages [31,32] and the recrystallization resistance of the irradiated materials. This will aid both in the appropriate grade selection for a fusion reactor and the design of healing processes enabling the lifetime extension of PFCs.

The recovery of tungsten in fusion relevant temperatures is segmented in different stages, based on the activation of different recovery mechanisms and can be summarized as follows: Monovacancy migration (from 400 to 600 °C) as stage III recovery [15,28,33–38], coalescence of small vacancy clusters, dislocation loop growth and dislocation line rearrangement (from 650 to 900 °C) as stage IV recovery [15,28,32,34,36–41], and finally complete defect recovery, heavily dependent on the irradiation conditions, sometimes termed as stage V recovery, observed at 900 °C [36], 1300 °C [15],1500 °C [32,37,42] and 1700 °C [43].

Recrystallization is an energy driven process, and the energy needed depends on the level of material deformation, and the resulting microstructural features such as grain size and impurities, as well as on radiation induced defects. For that reason, it is of no surprise that

recrystallization in non-irradiated tungsten is reported in the literature in a wide range of temperatures. From 1100 °C for 1 h [44], up to 1500 °C for 30 min [45] and everything in between [46-60]. However, the influence of neutron damage on the recrystallization behavior of W has not been addressed in the literature to the best of authors' knowledge.

In this work forged W bar and cold-rolled W plate, neutron irradiated to 0.18 displacements per atom (dpa) at 600 °C, have been isochronally annealed from 700 to 1550 °C for 24 h with a 50 °C step with two non–irradiated counterparts. The evolution of the microstructure is investigated through X-ray diffraction (XRD), optical microscopy, positron annihilation lifetime spectroscopy (PALS) and Vickers hardness. The evolution of the damage defects and the correlation between microstructure and hardening behavior are discussed, while the recovery stages of the two W grades are compared. By direct comparison of the two materials under the same annealing conditions information on the relative recrystallization resistance of the materials is provided.

2 Materials and Methods

2.1 Materials, neutron irradiation and annealing

The W materials were produced by PLANSEE SE in a powder metallurgical route consisting of sintering and hot forging from two orthogonal directions and subsequent stress-relief annealing at 1000 ^{o}C for 1h [54,61] (W forged bar) and of sintering, hot and cold-rolling (below 1200 °C) to a thickness of 1 mm [61,62] (W cold-rolled plate). Samples were cut, using Electrical Discharge Machining (EDM), in disk shape with a diameter of about 11 mm and were polished down to a thickness of about 0.5 mm. For the forged bar, the disks to be irradiated were cut with their surface normal to the axis of forging. For the non-irradiated samples of bar grade, specimens with their surface normal both along and perpendicular to the bar axis were cut. The samples were irradiated in the BR2 reactor (for which the typical spectra can be found in [63]), at SCK CEN at 600 °C for a duration of 70 days to a neutron fluence of about 9×10^{20} n/cm^2 for E>0.1 MeV corresponding to a dose of 0.18 displacements per atom (dpa), as determined by MCNPX 2.7.0 calculations using a threshold displacement energy of 55 eV. More details about the irradiation can be found in [64]. The irradiated microstructure contains dislocations, mainly in the form of loops, vacancy clusters and voids as well as transmutation products [25]. The Re, Os and Ta transmutation products have been evaluated by the FISPACT-II nuclide inventory code and employing TENDL-2019 nuclear library, for Re and Os, and EAF-2010 for Ta and they are found (0.54±0.06) at% Re, (0.013±0.002) at% Os and $(3.3\pm0.4)\times10^{-3}$ at% Ta. It is noted that EAF-2010 was used for the evaluation of the W transmutation into Ta because there is a better agreement of the experimental activities determined by gamma spectroscopy measurements with the calculated ones for EAF-2010 nuclear library.

The irradiated samples were post-irradiation annealed (PIA) under high vacuum for 24 h in the temperature range from 700 to 1550 °C with a 50 °C step. Non-irradiated W bar and cold-

rolled W (plate) samples were simultaneously annealed with the irradiated ones under the same conditions. All specimens, prior to annealing and irradiation, had been mechanically polished from both sides using sub-micron diamond suspension and colloidal silica for removing the surface damage caused by the manufacturing processes and/or EDM cutting.

From now on, the following terminology is used to differentiate the various sample conditions, a) *non-irradiated sample* refers to the initial state without irradiation and any heat treatment, b) *as irradiated sample* after the irradiation to 0.18 dpa at 600 °C and before any annealing, c) *post-irradiation annealed (PIA) sample* refers to the irradiated sample after annealing at a specific temperature (it is noted that the annealing at different temperatures is performed on the same sample) and d) *control sample* designates the non-irradiated sample annealed at different temperatures with the same conditions as the annealed irradiated sample.

2.2 Methods

2.2.1 Optical Microscopy

The grain structure of the control samples was probed through optical microcopy, using the upright Axio Imager 2 microscope by Zeiss. The available objective lenses range from a ×10 up to ×100 magnification.

2.2.2 XRD

The crystalline structure was evaluated by X-ray diffraction (XRD) measurements carried out at room temperature using a Bruker D8 diffractometer with a Cu Kα X-ray source, a parallel beam stemming from a Göbbel mirror and a scintillator detector.

2.2.3 PALS

Positron Annihilation Lifetime Spectroscopy measurements were carried out at room temperature, using the Ortec® PLS-system. A ^{22}Na radionuclide encapsulated in 3.6 mg/cm^2 thin polyimide (Kapton®) with an activity of 100 μCi was used as the positron source, sandwiched between two pieces of specimens. The detectors were placed in a linear configuration at a distance of about 3 mm from the sample. More details on the experimental setup and the analysis can be found in [64]. The data analysis was performed using LT10 software [65]. From the analysis of the data, the lifetime, τ_i, of each type i of defect and the probability, I_i, of the positron to be annihilated in type i defect ($\sum I_i = 1$) are determined.

2.2.4 Vickers Hardness

Vickers depth-sensing indentation experiments were performed employing a NANOVEA's mechanical tester. The maximum load was set at 3 N, while both the loading and the

unloading rate were set to 20 N/min. A dwell time of 200 s was applied before starting the unloading process. The loading rate was selected after a series of preliminary indentation tests to achieve stability in the hardness values. The holding time was chosen such as to attain equilibrium conditions, i.e. almost no change of the indentation depth. A set of six indentation tests, spaced by 200 μm, were performed for each measurement. An optical microscope was used to select the indented area free from visible defects.

3 Results and Discussion

3.1 Microstructure of the unirradiated and as-irradiated samples

The microstructure of the unirradiated and irradiated W forged bar and cold-rolled plate samples is described in [25,61]. The non-irradiated plate is characterized by grains elongated along the rolling direction with sub-grain size in the range of 1.5-2 μm. In the bar the grains are elongated along the bar axis, with sub-grain size varying in range from 0.6 to 1.7 μm and from 2.3 to 4 μm normal and along the bar axis respectively. The plate material has a much higher average dislocation density of $(9.8 \pm 2.0) \cdot 10^{13}$ m^{-2} compared to that of the bar being of about $(4\text{-}8) \cdot 10^{12}$ m^{-2} [25]. Dislocation loops can be observed in both materials. The bar contains loops in very low number density (below 10^{20} m^{-3}) but of very high size (exceeding 50 nm). In contrast the dislocation loops in the plate material exhibit a size of 3-11 nm with a number density of $6.3 \cdot 10^{19}$ m^{-3}. Both materials exhibit a high purity (> 99.97%), with the maximum and typical impurity elements as provided by the manufacturer presented in Table I.

Table I: Maximum and typical impurity contents of polycrystalline W bar and plate produced by Plansee SE.

Impurities	Al	Cr	Cu	Fe	K	Mo	Ni	Si	C	H	N	O	Cd	Hg	Pb
Maximum [μg/g]	15	20	10	30	10	100	20	20	30	5	5	20	5	1	5
Typical [μg/g]	1	3	1	8	1	12	2	1	6	-	1	2	1	-	1

After irradiation voids as well as dislocation loops and lines are formed in both materials, while the grain structure remains unaffected [25]. The voids have a density of $(4.1\pm1.1) \cdot 10^{22}$ m^{-3} for the bar and $(13\pm3) \cdot 10^{22}$ m^{-3} for the plate, with an average diameter of (1.4±0.3) nm for the bar and (1.2±0.7) nm for the plate. Dislocation loops are observed in the configuration of rafts or individual loops, having an average density of $(2.3\pm0.8) \cdot 10^{22}$ m^{-3} for the bar and $(2.1\pm0.9) \cdot 10^{22}$ m^{-3} for the plate, with an average diameter of (2.8±1.6) nm for the bar and (3.1±1.4) nm for the plate. The above mentioned errors refer to the standard deviation.

3.2 Optical Microscopy

Optical microscopy measurements were performed after each step of isochronal annealing on the control samples. Characteristic optical microscopy pictures after annealing for the control samples are presented in
Figure 1. After annealing at 1200 °C and 1300 °C for both W grades, grain boundary grooving [66–68] is observed revealing the underlying grain structure.

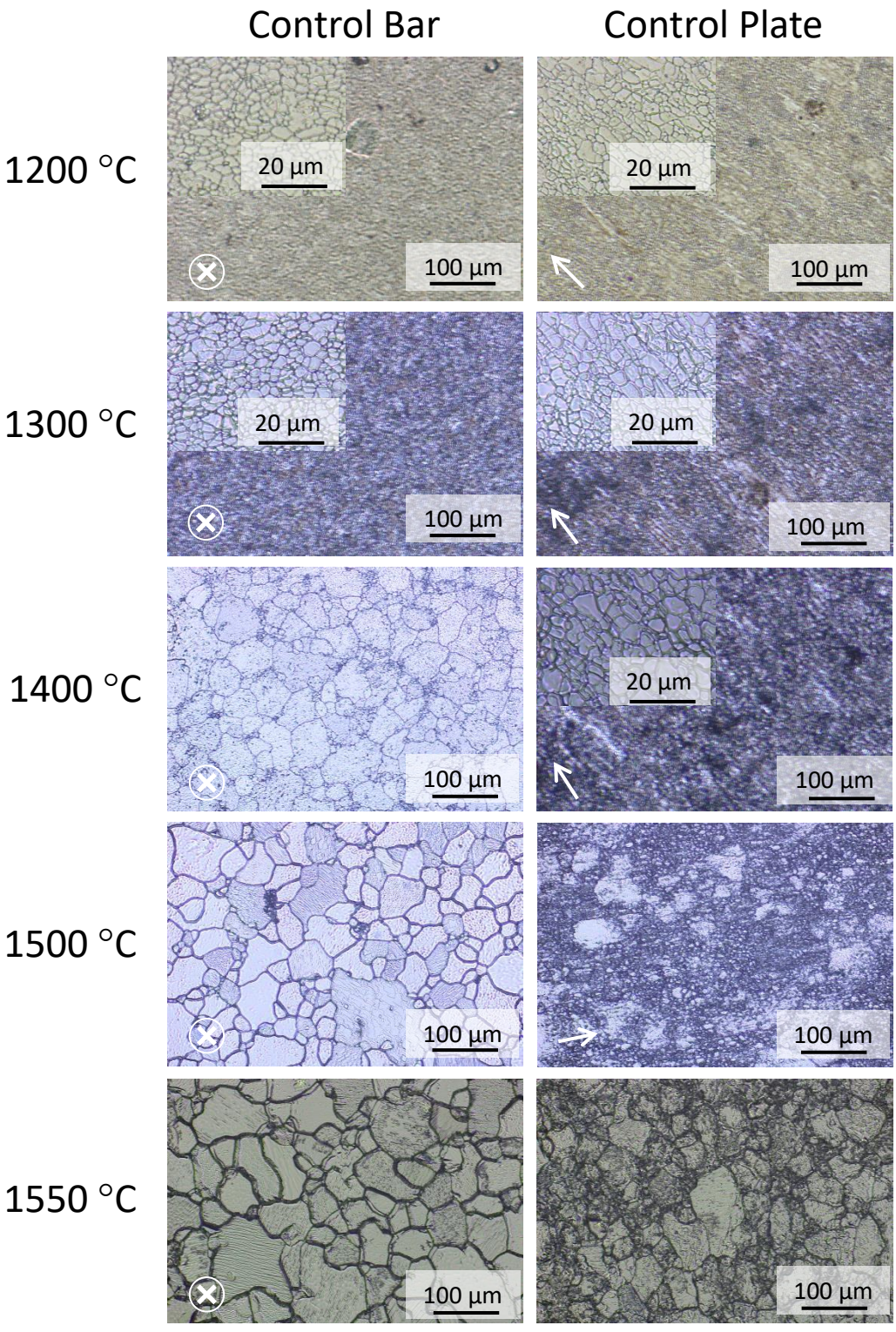

Figure 1: Optical microscopy images after characteristic annealing temperatures for the W control bar (left) and W control plate (right) samples. For the control bar the bar axis direction is shown, while in the case of the control plate, when apparent, the arrow shows the rolling direction of the plate.

The average grain size after annealing at 1200 °C, is measured to be (2.27 ± 0.09) μm for the bar and (1.80 ± 0.07) μm for the plate, in agreement with the sub-grain sizes determined by TEM in the original non irradiated samples [25], indicating that the sub-grains are visible after grain boundary grooving takes effect. After annealing at 1400 °C for the bar and 1500 °C for the plate, grain growth can be observed, with grains as large as ~100 μm in diameter, while some other grains remain unaffected. This difference in temperature reveals the increased recrystallization resistance of the plate compared to the bar. Further annealing leads to substantial grain growth, and annealing at 1550 °C results in the formation of grains with an average size of (50 ± 3) μm for the bar and (43 ± 3) μm for the plate.

3.3 XRD

X-ray diffraction measurements were performed after each step of isochronal annealing on both the irradiated and the control bar and plate samples. In order to assess recrystallization, the evolution of the texture coefficient (TC) for the bar (Figure 2) and plate (Figure 3) after isochronal annealing for both the control and post-irradiated samples is used. The texture coefficient of a crystallographic plane $(hkl)_i$ is defined as:

$$T_c(hkl)_i = \frac{\frac{I(hkl)_i}{I_0(hkl)_i}}{\frac{1}{N}\sum_{i=1}^{N}\frac{I(hkl)_i}{I_0(hkl)_i}} \quad (1)$$

where $I(hkl)_i$ is the observed intensity of the peak corresponding to the $(hkl)_i$ crystallographic plane, $I_0(hkl)_i$ is the intensity of the same peak for a randomly oriented polycrystalline sample and N is the total number of visible peaks. A texture coefficient having a value of 1 corresponds to randomly orientated crystallites in the sample, while a value higher (lower) than 1 indicates a (non-)preference in the specific crystallographic direction.

For the control bar and plate, signs of recrystallization start appearing after annealing at 1300 and 1400 °C, respectively, with a drastic change of texture of the (222) Bragg peak for the bar and an increase in intensity in the already strong (200) component for the plate.

Regarding the irradiated plate, the drastic increase of the (200) TC after PIA at 1500 °C (Figure 3) could indicate the onset of recrystallization, but could still be attributed to extended recovery, with only small adjustments in the sub-grain boundaries sharpening the texture of the deformed material [69]. For the irradiated bar (Figure 2), the small differences

in the determined texture is due to the inhomogeneity of the material's texture in the plane normal to the bar axis. However, after PIA at 1400 °C the decrease of the TC for (110) Bragg peak and the increase of that for (222) Bragg peak could indicate recrystallization.

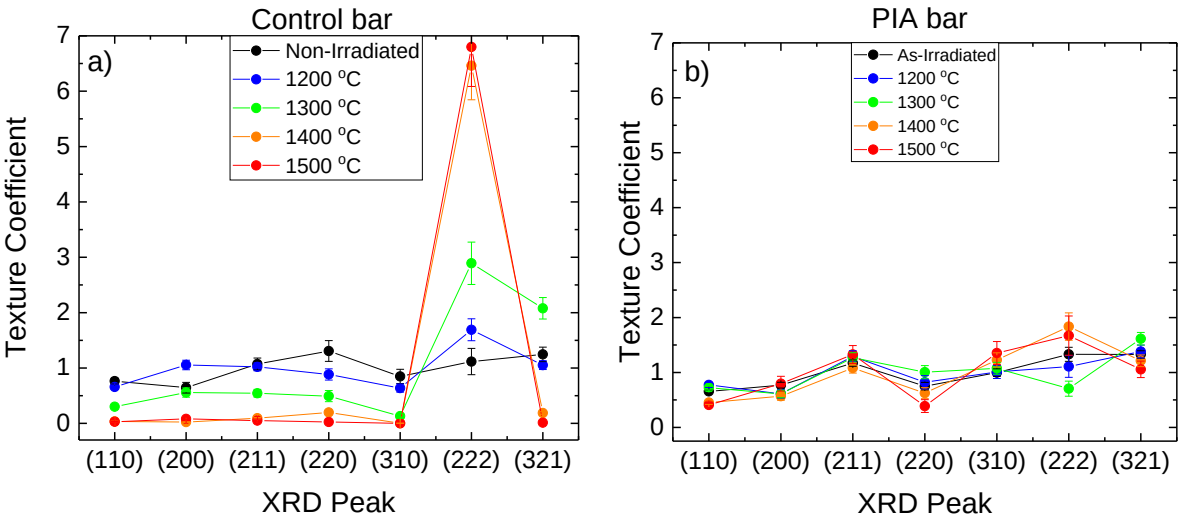

Figure 2: Texture coefficient for the various Bragg peaks after representative steps of annealing (a) and PIA (b) for the control and irradiated to 0.18 dpa at 600 °C W bar samples, respectively.

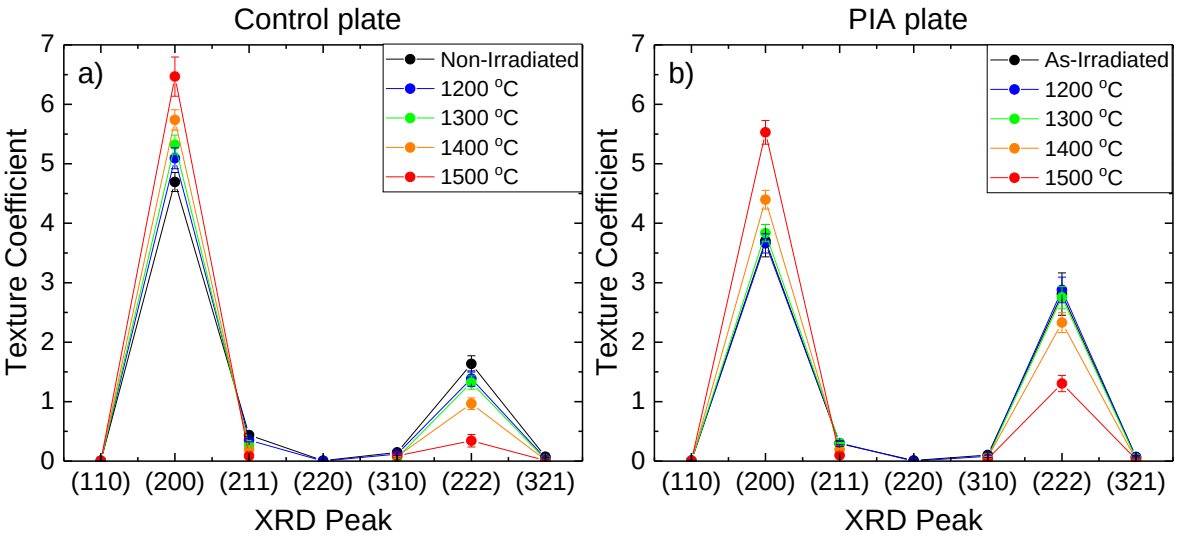

Figure 3: Texture coefficient for the various Bragg peaks after representative steps of annealing (a) and PIA (b) for the control and irradiated to 0.18 dpa at 600 oC W plate samples, respectively.

3.4 Open volume defects from PALS

In both W bar and plate control samples, one positron lifetime, τ, is required to describe the PALS spectra, having a value of (152±1) ps for the bar and (159±6) ps for the plate (Figure 4). This lifetime is a compound time, considered as a weighted average of lifetimes for annihilations taking place in the defect-free bulk (100-116 ps), in dislocations (130-180 ps) and possibly in mono-vacancies (160-200 ps) ([64] and references therein). The plate being

more heavily deformed compared to the bar shows a slightly higher lifetime than the bar due to the much higher number density of dislocations.

The evolution of the positron lifetime, τ, after annealing of the control samples is depicted in Figure 4. An increase of τ after annealing at 700 °C (800 °C) for the bar (plate) is observed which is attributed to the emission of vacancies bound at dislocations or impurities, increasing the effective positron lifetime. The difference in temperature needed for the detrapping of vacancies between the two materials types could be mainly due to the different dislocation structures emerging from the different fabrication processes, i.e. forging and rolling, ultimately altering the energy needed for the specific mechanism to be activated. After annealing at 850 °C for both materials the positron lifetime lies between 160 and 150 ps, a range indicative of positron annihilations in dislocations and continues dropping to values below 150 ps upon further annealing at 950 °C for the bar and 1150 °C for the plate, signifying a reduction in the dislocation density and increase of positron annihilation in the defect free part of the tungsten. A major decrease in the positron lifetime after annealing at 1300 °C (1400 °C) for the bar (plate) could be an indication of recrystallization, with the lifetime attaining values in the region of a pristine W(100) single crystal (114 ps) [70] after annealing at 1400 °C (1550 °C) for the bar (plate), showing that the majority of the positron annihilations take place in the defect free part of the material.

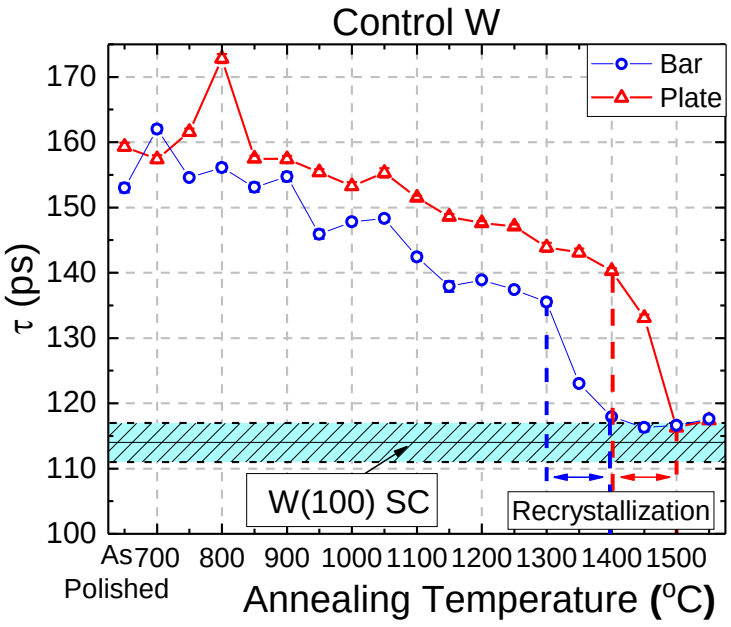

Figure 4: Evolution of positron annihilation lifetime as determined by PALS, after each step of isochronal annealing, for the control W Bar (○) and the W plate (△). The positron annihilation lifetime of the W(100) single crystal (SC) [32] *is also shown for reference. The dashed vertical lines show the recrystallization region for each material type.*

After irradiation two positron lifetimes are needed to simulate the PALS spectra for both W grades, a short one, τ_1, and a long one, τ_2. The short lifetime attains an increased value, compared to the non-irradiated sample, of (168±2) ps for the bar (Figure 5a) and (164±3) ps

for the plate (Figure 6a), indicative of the creation of irradiation induced dislocations in the material. The long lifetime, τ_2,corresponds to annihilations in vacancy clusters or voids (with more than 40 vacancies) having a diameter larger than 1 nm, for which theoretical calculations predict a small or no dependence of the positron lifetime on the void size due to the localization of positron at the void surface, with a saturation positron lifetime value of around 500 ps [71,72]. The similar lifetimes determined for both the irradiated bar and plate materials are a testament to the same types of irradiation induced defects present in the materials.

The determined positron lifetimes and the corresponding intensities of the PIA samples for the bar and plate samples are presented in Figures 5 and 6, respectively. Up to PIA at 1150 ^{o}C, for both the bar and the plate (Figures 5a and 6a), τ_1 remains almost constant, while a continuous decrease is observed afterwards up to annealing at 1550 °C. Since τ_1 is a weighted average, as described above, this decrease, corresponding to a reduction of the contribution of positron annihilations in dislocations, indicates dislocation annihilation. It should be noted that both W grades do not attain the lifetimes values of a pristine W(100) single crystal in contrast to their control counterparts, after annealing at 1550 °C. This indicates that while recrystallization and grain growth have taken place, there are still a number of grain boundaries trapping positrons, slightly elevating the positron lifetime. This inference is supported by our previous study regarding the annealing of a neutron irradiated single crystal W to a similar dose [32], in which recrystallization does not occur, where after annealing at 1500 °C τ_1 reaches the value of a pristine W(100) single crystal.

The long positron lifetime (Figures 5a and 6a), τ_2, is found to increase in two stages, directly after PIA up to 750 °C and after PIA in the range of 950 – 1150 °C. The first increase is related to de-trapping of vacancies and their subsequent coalescence leading to the increase of the average size of vacancy clusters. The second regime of increased τ_2 is attributed to excessive void growth involving, most probably, an Ostwald ripening process [73]. It is noted that positron lifetimes larger than 500 ps, which are above the theoretical saturation value of 420 ps, have been attributed to pick-off annihilations of ortho-positronium formed in large vacancy clusters [15,37], suggesting that the internal surfaces of the clusters may be partially decorated with impurities [15]. Therefore, the positron lifetime values for the voids found in the current study may be also related to the segregation of Re/Os at the void surface, which was evidenced by other experiments at a higher irradiation dose [74,75]. However, due to a higher positron affinity to W-vacancy than Re/Os-vacancy [76], positron annihilation spectroscopy is not sensitive towards possible Re/Os-vacancy clusters.

Regarding the relative intensities of the components, the following reasoning can be made. The relative intensity is proportional to the trapping rate, κ, of the defect, which is equal to the defect number density, N, multiplied by the trapping strength, μ, of the defect ($I \propto \kappa = \mu N$) [77]. The increase in the relative intensity of the long lifetime (Figures 5b and 6b), I_2, for both grades from 950 to 1100 °C, is indicative of both the reduction of the dislocation density and the increase in the trapping strength of the voids with increasing void

size. The coalescence of vacancy clusters into larger voids seems to increase the void trapping rate, regardless of the decrease in their number density. The decrease in the relative intensity after 1150 °C for the polycrystalline materials and onwards could be attributed to void dissolution, with complete void dissolution observed after annealing at 1450 °C and 1400 °C for the bar and plate, respectively.

The systematic dominance of the intensity of the positron lifetime attributed to dislocations (I_1) over the one attributed to voids (I_2) for both materials reflects the fact that dislocations mainly shape the PALS spectrum. This observation allows one to attribute the systematically higher intensity of about 5% for the dislocation component (I_1) in the irradiated plate compared to the bar, to a higher total dislocation density of the plate, however not in absolute values, after irradiation.

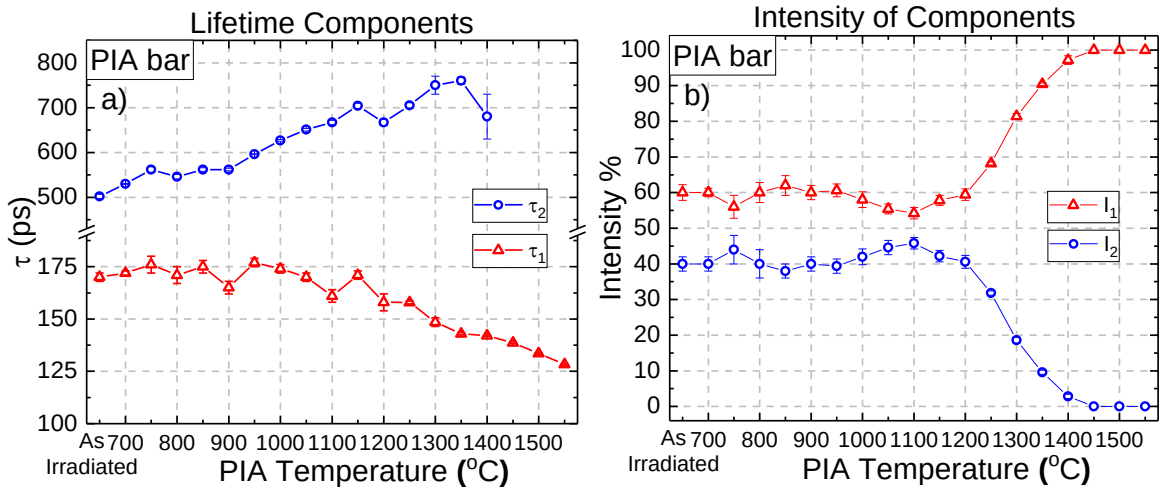

Figure 5: Positron annihilation lifetimes, τ_1 (△) and τ_2 (○) (a) and their relative intensities I_1 (△) and I_2 (○) (b) as determined by PALS, after each step of PIA for the irradiated to 0.18 dpa at 600 °C W bar sample.

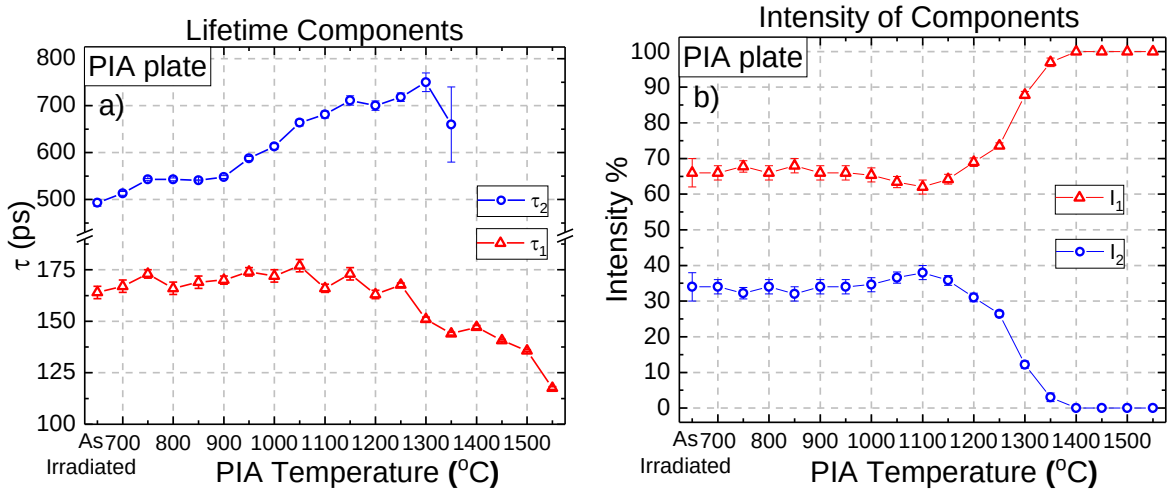

Figure 6: Positron annihilation lifetimes, τ_1 (△) and τ_2 (○) (a) and their relative intensities I_1 (△) and I_2 (○) (b) as determined by PALS, after each step of PIA for the irradiated to 0.18 dpa at 600 °C W Plate sample.

3.5 Vickers Hardness

Vickers hardness measurements were performed after each step of isochronal annealing on both the irradiated and the control samples. The determined Vickers hardness after each step of isochronal annealing of both the control and PIA samples is presented in Figure 7.

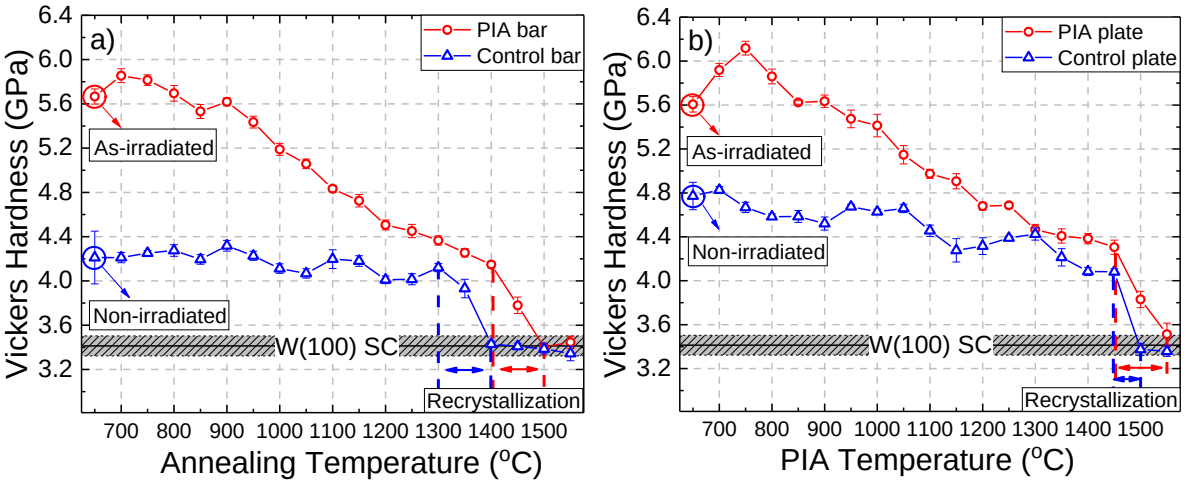

Figure 7: Vickers hardness after each step of isochronal annealing of the control and irradiated to 0.18 dpa at 600 °C W bar (a) and W plate (b) samples. The temperature ranges where recrystallization occurs are highlighted. The hardness of the W(100) single crystal (SC) is from [32]. *The dashed vertical lines show the recrystallization region for each material type.*

Comparing the non-irradiated samples, the plate presents the highest hardness, (4.7±0.1) GPa versus (4.2±0.2) GPa for the bar, due to the higher initial degree of deformation compared to the W bar. However, after irradiation, both W grades present similar hardness values.

Regarding the hardness evolution of the control bar (Figure 7a) a first region of hardness decrease of about 0.3 GPa is observed in the temperature range from 950 to 1350 °C, reflecting dislocation annihilation, followed by a sudden drop after annealing at 1400 °C to the value of non-irradiated single crystal [32] indicating that recrystallization and grain growth have taken place.

For the control plate (Figure 7b) an initial small decrease of about 0.4 GPa (with respect to the non-irradiated state) is observed after annealing at 900 °C , a second one of 0.2 GPa after annealing at 1150 °C, and a third one after annealing at 1400 °C. The first two drops are attributed to dislocation annihilation while the third one to extended recovery – adjustments in the sub-grain boundaries [69]. The onset of dislocation recovery takes place at a lower temperature in the plate than in the bar because of the much higher dislocation density of the former. Besides, recovery of the bar has already taken effect from the stress-relief annealing at 1000 °C for 1 h following forging. The initial part of the dislocation recovery observed in the plate near 900 °C has already occurred in the bar, also evident from the much lower dislocation density of the latter. Finally after annealing at 1500 °C the Vickers hardness reaches the value of the non-irradiated single crystal, signaling that recrystallization and grain growth have taken place.

Regarding the irradiated samples the following behaviour is observed after PIA. An initial increase in hardness with a peak at 700 °C for the bar (Figure 7a) and at 750 °C for the plate (Figure 7b) is apparent, followed by an almost continuous decrease. For the irradiated bar (Figure 7a) two discrete recovery ranges can be identified: one from 900 °C to 1200 °C with a decrease in hardness of about 4MPa/°C, and another from 1200 °C to 1400 °C with a decrease in hardness of about 2MPa/°C. For the irradiated plate, the hardness recovery is rather continuous from 900 to 1300 °C, with a rate of 3 MPa/°C presenting no discrete identifiable ranges. The initial increase in hardness is attributed to monovacancy detrapping from impurities and vacancy cluster formation-growth and is more pronounced in the plate material, as is the case for the non-irradiated samples as well, as evidenced by PALS (Figure 4). The plate reaches the non-irradiated reference hardness value after annealing at 1150 °C, while for the bar this takes place after annealing at 1350 °C. The decrease in hardness from 900 °C and onwards is attributed to both vacancy cluster coarsening and dislocation annihilation. Finally, a last decrease in hardness from 1400 to 1500 °C for the bar and from 1450 to 1550 °C for the plate at a rate of roughly 8 MPa/°C indicates grain growth. Both the irradiated bar and plate samples reach the hardness value of the non-irradiated single crystal W, revealing that significant grain growth has occurred. From this, one may infer that there is no formation of a significant number of precipitates or clusters of transmutation products, since these would cause an observable impact on the measured hardness.

A quantitative way of comparing recrystallization resistance would be using the temperature dependent time to half recrystallization [45,48,55,78–81]. However, a representative recrystallization temperature (for 24 h annealing) corresponding to half of the hardening loss from recrystallization can be used [79] and this is presented in Table II.

Table II: Recrystallization temperature for 24 h annealing, defined as the temperature where half of the hardening loss from recrystallization has occurred, for the non-irradiated and irradiated to 0.18 dpa at 600 °C W forged bar and W cold-rolled plate.

Recrystallization temperature for 24 h annealing	Forged bar	Cold-rolled plate
Non-irradiated	1375 °C	1475 °C
Irradiated to 0.18 dpa at 600 °C	1450 °C	1500 °C

Comparing the recrystallization temperature of the non-irradiated W grades, the higher initial deformation of the plate seems to provide a higher resistance to recrystallization compared to the bar.
Since recrystallization depends on the stored energy in a material, one would expect that the more highly deformed material would recrystallize faster. However that does not seem to be the case. Behind this discordance the following three factors could contribute on different degrees:

1) Recovery depends on the stored energy in a material and is antagonizing to recrystallization. Therefore the recovery in hardness observed after annealing in the plate may lead to a higher reduction of the stored energy compared to the bar, resulting in the retardation of recrystallization. Especially the extended recovery – adjustments in the sub-grain boundaries [69] in the plate, which are absent in the bar, could contribute heavily towards the observed phenomenon.
2) The difference in grain structure between the two materials, while small, could play a major role in the recrystallization kinetics. TEM revealed that the sub-grain size in the bar material is slightly smaller compared to the plate, which in turn means that there are more possible nucleation sites for new grains in the bar, facilitating and speeding recrystallization. Also, the difference in initial texture (almost textureless bar and strong (100) and (222) textured plate) could also influence recrystallization [82].
3) Different impurity levels in the two W grades could influence recrystallization kinetics, with some impurity atoms pinning the grain boundaries and retarding recrystallization even in small concentrations, or even forming bubbles retarding boundary motion through Zener pinning forces, as is the case in the well-studied K-doped W [47,83,84].

After irradiation, the recrystallization resistance of both grades increases, with the plate presenting a recrystallization temperature (as defined above) higher than that of the bar by about 50 °C.

4 Summary and Conclusions

Tungsten in plate and bar form, produced by PLANSEE SE in a powder metallurgical route consisting of sintering and rolling and hot forging from two orthogonal directions were

irradiated in the BR2 reactor, at SCK CEN, to 0.18 dpa at 600 °C. Annealing of the irradiated samples together with non-irradiated ones was performed under high vacuum isochronally for 24 hours, in the temperature range 700 to 1550 °C in steps of 50 °C.

The two tungsten grades studied, due to the difference in their manufacturing process, present dissimilarities in their microstructure. Despite the similar sub-grain sizes of roughly ~1 μm, their textures differ drastically with the plate having a strong (100) and (222) texture and the bar being almost textureless. The difference in their deformation levels leads to a significant difference in their dislocation densities with the plate exhibiting more than 10 times higher dislocation density compared to the bar. The stress relief annealing of the bar after forging at 1000 °C for 1 h contributes heavily to this difference as well. All the above are the main factors contributing to the differences in both recovery and recrystallization kinetics between the two grades which are summarized below.

Recovery of the non-irradiated bar and plate is rather continuous with dislocation re-arrangement, rotation and annihilation occurring after annealing at 900 °C for the bar and after annealing at 700 °C for the plate. Vacancy emission seems to occur at 700 °C for the bar and 800 °C for the plate. The plate presents extended recovery with further sharpening of the characteristic (200) texture after annealing at 1300 °C, before recrystallizing.

Regarding the irradiated samples more recovery stages are apparent for both grades with the de-trapping of vacancies, leading to their coalescence, around 750 °C, followed by vacancy cluster coarsening as well as dislocation annihilation from 900 °C onwards and lastly Ostwald ripening in the range of 950 to 1150 °C. Void dissolution begins after annealing at 1150 °C for both grades resulting in a void – free microstructure after PIA at 1450 °C for the bar and 1400 °C for the plate.

All the techniques used in the present study demonstrate the higher recrystallization resistance of the plate compared to the bar before and after neutron irradiation to 0.18 dpa at 600 °C. Neutron irradiation seems to increase the recrystallization resistance of both W grades, especially for the bar. To the best of the authors' knowledge, the present study is novel with regard to the effect of irradiation on recrystallization kinetics, with works in the literature focusing on the effects of different fusion related phenomena, such as the effect of He exposure[85–89], Ne irradiation [90] and H exposure[91].

Therefore, concerning the effect of the initial microstructure on annealing and recrystallization kinetics on two ITER specification W grades, and their possible use in a fusion reactor, the plate material appears to be more promising compared to the bar. Besides the lower irradiation hardening the plate presents the advantage that void dissolution occurs before recrystallization, meaning that an annealing regime exists where a large part of the irradiation damage is healed while softening from recrystallization is avoided. Consequently, while this annealing range is quite narrow, it could pave the way towards an in-situ annealing cycle prolonging the lifetime of the in-vessel plasma facing components.

Acknowledgments

This work has been carried out within the framework of the EUROfusion Consortium, funded by the European Union via the Euratom Research and Training Programme (Grant Agreement Nos 633053 and 101052200 — EUROfusion). Views and opinions expressed are however those of the author(s) only and do not necessarily reflect those of the European Union or the European Commission. Neither the European Union nor the European Commission can be held responsible for them. The funding from the Hellenic General Secretariat for Research and Innovation for the Greek National Programme of the Controlled Thermonuclear Fusion is acknowledged.

References

[1] H. Bolt, V. Barabash, W. Krauss, J. Linke, R. Neu, S. Suzuki, N. Yoshida, Materials for the plasma-facing components of fusion reactors, J. Nucl. Mater. 329–333 (2004) 66–73. https://doi.org/10.1016/j.jnucmat.2004.04.005.

[2] R.A. Pitts, S. Carpentier, F. Escourbiac, T. Hirai, V. Komarov, S. Lisgo, A.S. Kukushkin, A. Loarte, M. Merola, A. Sashala Naik, R. Mitteau, M. Sugihara, B. Bazylev, P.C. Stangeby, A full tungsten divertor for ITER: Physics issues and design status, J. Nucl. Mater. 438 (2013) S48--S56. https://doi.org/10.1016/j.jnucmat.2013.01.008.

[3] G. Pintsuk, Tungsten as a Plasma-Facing Material, in: Compr. Nucl. Mater., Elsevier, Amsterdam, The Netherlands, 2012: pp. 551–581. https://doi.org/10.1016/B978-0-08-056033-5.00118-X.

[4] J.W. Davis, V.R. Barabash, A. Makhankov, L. Plöchl, K.T. Slattery, Assessment of tungsten for use in the ITER plasma facing components, J. Nucl. Mater. 258–263 (1998) 308–312. https://doi.org/10.1016/S0022-3115(98)00285-2.

[5] V. Philipps, Tungsten as material for plasma-facing components in fusion devices, J. Nucl. Mater. 415 (2011) S2--S9. https://doi.org/10.1016/j.jnucmat.2011.01.110.

[6] J.H. Yu, H. Tanigawa, D. Hamaguchi, T. Nozawa, Mechanical properties of three kinds of ITER-Grade pure tungsten with different manufacturing processes, Fusion Eng. Des. 157 (2020) 111679. https://doi.org/10.1016/j.fusengdes.2020.111679.

[7] J. Reiser, J. Hoffmann, U. Jäntsch, M. Klimenkov, S. Bonk, C. Bonnekoh, M. Rieth, A. Hoffmann, T. Mrotzek, Ductilisation of tungsten (W): On the shift of the brittle-to-ductile transition (BDT) to lower temperatures through cold rolling, Int. J. Refract. Met. Hard Mater. 54 (2016) 351–369. https://doi.org/10.1016/J.IJRMHM.2015.09.001.

[8] C. Bonnekoh, A. Hoffmann, J. Reiser, The brittle-to-ductile transition in cold rolled tungsten: On the decrease of the brittle-to-ductile transition by 600 K to − 65 °C, Int. J. Refract. Met. Hard Mater. 71 (2018) 181–189. https://doi.org/10.1016/j.ijrmhm.2017.11.017.

[9] C. Yin, D. Terentyev, T. Pardoen, A. Bakaeva, R. Petrov, S. Antusch, M. Rieth, M. Vilémová, J. Matějíček, T. Zhang, Tensile properties of baseline and advanced tungsten grades for fusion applications, Int. J. Refract. Met. Hard Mater. 75 (2018) 153–162. https://doi.org/10.1016/j.ijrmhm.2018.04.003.

[10] O. Motojima, The ITER project construction status, Nucl. Fusion. 55 (2015) 104023. https://doi.org/10.1088/0029-5515/55/10/104023.

[11] R.C. Rau, R.L. Ladd, J. Moteff, Voids in irradiated tungsten and molybdenum, J. Nucl. Mater. 33 (1969) 324–327. https://doi.org/10.1016/0022-3115(69)90029-4.

[12] M. Rieth, S.L. Dudarev, S.M. Gonzalez De Vicente, J. Aktaa, T. Ahlgren, S. Antusch, D.E.J. Armstrong, M. Balden, N. Baluc, M.F. Barthe, W.W. Basuki, M. Battabyal, C.S. Becquart, D. Blagoeva, H. Boldyryeva, J. Brinkmann, M. Celino, L. Ciupinski, J.B. Correia, A. De Backer, C. Domain, E. Gaganidze, C. García-Rosales, J. Gibson, M.R. Gilbert, S. Giusepponi, B. Gludovatz, H. Greuner, K. Heinola, T. Höschen, A. Hoffmann, N. Holstein, F. Koch, W. Krauss, H. Li, S. Lindig, J. Linke, C. Linsmeier, P. López-Ruiz, H. Maier, J. Matejicek, T.P. Mishra, M. Muhammed, A. Muñoz, M. Muzyk, K. Nordlund, D. Nguyen-Manh, J. Opschoor, N. Ordás, T. Palacios, G. Pintsuk, R. Pippan, J. Reiser, J. Riesch, S.G. Roberts, L. Romaner, M. Rosiński, M. Sanchez, W. Schulmeyer, H. Traxler, A. Ureña, J.G. Van Der Laan, L. Veleva, S. Wahlberg, M. Walter, T. Weber, T. Weitkamp, S. Wurster, M.A. Yar, J.H. You, A. Zivelonghi, Recent progress in research on tungsten materials for nuclear fusion applications in Europe, J. Nucl. Mater. 432 (2013) 482–500. https://doi.org/10.1016/j.jnucmat.2012.08.018.

[13] J.T. Buswell, Vacancy damage in heavy ion and neutron-irradiated tungsten, Philos. Mag. 22 (1970) 787–802. https://doi.org/10.1080/14786437008220947.

[14] J.A. Brinkman, On the Nature of Radiation Damage in Metals, J. Appl. Phys. 25 (1954) 961–970. https://doi.org/10.1063/1.1721810.

[15] X. Hu, T. Koyanagi, M. Fukuda, Y. Katoh, L.L. Snead, B.D. Wirth, Defect evolution in single crystalline tungsten following low temperature and low dose neutron irradiation, J. Nucl. Mater. 470 (2016) 278–289. https://doi.org/10.1016/j.jnucmat.2015.12.040.

[16] O. V. Ogorodnikova, M. Majerle, J. Čížek, S. Simakov, V. V. Gann, P. Hruška, J. Kameník, J. Pospíšil, M. Štefánik, M. Vinš, Positron annihilation spectroscopy study of radiation-induced defects in W and Fe irradiated with neutrons with different spectra, Sci. Rep. 10 (2020) 1–13. https://doi.org/10.1038/s41598-020-75737-8.

[17] M.R.R. Gilbert, J.-C. Sublet, Neutron-induced transmutation effects in W and W-alloys in a fusion environment, Nucl. Fusion. 51 (2011) 43005. https://doi.org/10.1088/0029-5515/51/4/043005.

[18] M. Klimenkov, U. Jäntsch, M. Rieth, H.C.C. Schneider, D.E.J.E.J. Armstrong, J. Gibson, S.G.G. Roberts, Effect of neutron irradiation on the microstructure of tungsten, Nucl. Mater. Energy. 9 (2016) 480–483. https://doi.org/10.1016/j.nme.2016.09.010.

[19] M.J. Lloyd, R.G. Abernethy, M.R. Gilbert, I. Griffiths, P.A.J.J. Bagot, D. Nguyen-Manh, M.P. Moody, D.E.J.J. Armstrong, Decoration of voids with rhenium and osmium transmutation products in neutron irradiated single crystal tungsten, Scr. Mater. 173 (2019) 96–100. https://doi.org/10.1016/j.scriptamat.2019.07.036.

[20] A. Hasegawa, M. Fukuda, K. Yabuuchi, S. Nogami, Neutron irradiation effects on the microstructural development of tungsten and tungsten alloys, J. Nucl. Mater. 471 (2016) 175–183. https://doi.org/10.1016/j.jnucmat.2015.10.047.

[21] V.K. Sikka, J. Moteff, Superlattice of voids in neutron-irradiated tungsten, J. Appl. Phys. 43 (1972) 4942–4944. https://doi.org/10.1063/1.1661050.

[22] M. Fukuda, K. Yabuuchi, S. Nogami, A. Hasegawa, T. Tanaka, Microstructural

development of tungsten and tungsten-rhenium alloys due to neutron irradiation in HFIR, J. Nucl. Mater. 455 (2014) 460–463. https://doi.org/10.1016/j.jnucmat.2014.08.002.

[23] M. Fujitsuka, B. Tsuchiya, I. Mutoh, T. Tanabe, T. Shikama, Effect of neutron irradiation on thermal diffusivity of tungsten–rhenium alloys, J. Nucl. Mater. 283–287 (2000) 1148–1151. https://doi.org/10.1016/S0022-3115(00)00170-7.

[24] L.M.M. Garrison, Y. Katoh, N.A.P.K.A.P.K. Kumar, Mechanical properties of single-crystal tungsten irradiated in a mixed spectrum fission reactor, J. Nucl. Mater. 518 (2019) 208–225. https://doi.org/10.1016/j.jnucmat.2019.02.050.

[25] A. Dubinko, D. Terentyev, C. Yin, W. Van Renterghem, B. Rossaert, M. Rieth, E.E.E. Zhurkin, A. Zinovev, C.C.C. Chang, S. Van Dyck, G. Bonny, Microstructure and hardening induced by neutron irradiation in single crystal, ITER specification and cold rolled tungsten, Int. J. Refract. Met. Hard Mater. 98 (2021) 105522. https://doi.org/10.1016/j.ijrmhm.2021.105522.

[26] B. Wielunska, T. Płociński, T. Schwarz-Selinger, M. Mayer, W. Jacob, L. Ciupiński, Dislocation structure of tungsten irradiated by medium to high-mass ions, Nucl. Fusion. 62 (2022) 096003. https://doi.org/10.1088/1741-4326/ac75ff.

[27] C.L. Dube, P.K. Kulriya, D. Dutta, P.K. Pujari, Y. Patil, M. Mehta, P. Patel, S.S. Khirwadkar, Positron annihilation lifetime measurement and X-ray analysis on 120 MeV Au+7 irradiated polycrystalline tungsten, J. Nucl. Mater. 467 (2015) 406–412. https://doi.org/10.1016/j.jnucmat.2015.05.029.

[28] J. Grzonka, Ł. Ciupiński, J. Smalc-Koziorowska, O.V. Ogorodnikova, M. Mayer, K.J. Kurzydłowski, Electron microscopy observations of radiation damage in irradiated and annealed tungsten, Nucl. Instruments Methods Phys. Res. Sect. B Beam Interact. with Mater. Atoms. 340 (2014) 27–33. https://doi.org/10.1016/j.nimb.2014.07.043.

[29] X. Yi, M.L. Jenkins, M.A. Kirk, Z. Zhou, S.G. Roberts, In-situ TEM studies of 150 keV W+ ion irradiated W and W-alloys: Damage production and microstructural evolution, Acta Mater. 112 (2016) 105–120. https://doi.org/10.1016/j.actamat.2016.03.051.

[30] X. Yi, M.L. Jenkins, M. Briceno, S.G. Roberts, Z. Zhou, M.A. Kirk, In situ study of self-ion irradiation damage in W and W-5Re at 500°C, Philos. Mag. 93 (2013) 1715–1738. https://doi.org/10.1080/14786435.2012.754110.

[31] D. Papadakis, K. Mergia, E. Manios, V. Chatzikos, S. Dellis, D. Terentyev, G. Bonny, W. Van Renterghem, C.C. Chang, S. Messoloras, Defect evolution of neutron irradiated ITER grade tungsten after annealing, Fusion Eng. Des. 189 (2023) 113486. https://doi.org/10.1016/j.fusengdes.2023.113486.

[32] D. Papadakis, K. Mergia, E. Manios, V. Chatzikos, S. Dellis, S. Messoloras, Post neutron irradiation annealing and defect evolution in single crystal tungsten, Nucl. Mater. Energy. 34 (2023) 101357. https://doi.org/10.1016/j.nme.2022.101357.

[33] P.E. Lhuillier, M.F. Barthe, P. Desgardin, W. Egger, P. Sperr, Positron annihilation studies on the nature and thermal behaviour of irradiation induced defects in tungsten, Phys. Status Solidi. 6 (2009) 2329–2332. https://doi.org/10.1002/pssc.200982114.

[34] B. Horvath, Y. Dai, Y. Lee, Annealing effect on the microstructure of tungsten irradiated in SINQ target, J. Nucl. Mater. 506 (2018) 19–25. https://doi.org/10.1016/J.JNUCMAT.2017.12.020.

[35] P.M.G.G. Nambissan, P. Sen, Positron annihilation study of the annealing behaviour of

alpha induced defects in tungsten, Radiat. Eff. Defects Solids. 124 (1992) 215–221. https://doi.org/10.1080/10420159208220193.

[36] O.V. Ogorodnikova, L.Y. Dubov, S.V. Stepanov, D. Terentyev, Y.V. Funtikov, Y.V. Shtotsky, V.S. Stolbunov, V. Efimov, K. Gutorov, Annealing of radiation-induced defects in tungsten: Positron annihilation spectroscopy study, J. Nucl. Mater. 517 (2019) 148–151. https://doi.org/10.1016/j.jnucmat.2019.02.010.

[37] M. Zibrov, W. Egger, J. Heikinheimo, M. Mayer, F. Tuomisto, Vacancy cluster growth and thermal recovery in hydrogen-irradiated tungsten, J. Nucl. Mater. 531 (2020) 152017. https://doi.org/10.1016/j.jnucmat.2020.152017.

[38] O.V. Ogorodnikova, Y. Gasparyan, V. Efimov, Ł. Ciupiński, J. Grzonka, Annealing of radiation-induced damage in tungsten under and after irradiation with 20MeV self-ions, J. Nucl. Mater. 451 (2014) 379–386. https://doi.org/10.1016/j.jnucmat.2014.04.011.

[39] A. Chauhan, Q. Yuan, D. Litvinov, E. Gaganidze, H.C. Schneider, D. Terentyev, J. Aktaa, Effect of temperature on the neutron irradiation-induced cavities in tungsten, Philos. Mag. 102 (2022) 1665–1683. https://doi.org/10.1080/14786435.2022.2079750.

[40] P.M.G. Nambissan, P. Sen, Positron annihilation study of the annealing behaviour of alpha induced defects in tungsten, Radiat. Eff. Defects Solids. 124 (1992) 215–221. https://doi.org/10.1080/10420159208220193.

[41] F.L. Article, Y. Yuan, S. Wang, S. Wang, W. Guo, H. Wang, X. Yi, L. Ge, Y. Sun, L. Cheng, X. Zhang, Y. Yuan, X. Cao, E. Fu, G. Lu, T. Schwarz-selinger, S. Scientist, Journal of Nuclear Materials Defect annealing in heavy-ion irradiated tungsten : Long-time thermal evolution of saturated displacement damage at different temperatures, J. Nucl. Mater. 581 (2023) 154454. https://doi.org/10.1016/j.jnucmat.2023.154454.

[42] M.I. Zakharova, N.A. Artemov, V. V. Bogdanov, Effects of neutron irradiation and annealing on the elastic moduli and electrical resistivity of molybdenum and tungsten single crystals, Inorg. Mater. 37 (2001) 786–789. https://doi.org/10.1023/A:1017979230262.

[43] M. Zibrov, T. Dürbeck, W. Egger, M. Mayer, High temperature recovery of radiation defects in tungsten and its effect on deuterium retention, Nucl. Mater. Energy. 23 (2020) 100747. https://doi.org/10.1016/j.nme.2020.100747.

[44] Z.S. Levin, B.G. Brady, D.C. Foley, K.T. Hartwig, Recrystallization behavior of tungsten processed by equal channel angular extrusion at low homologues temperature: Microstructure, hardness, and texture, Int. J. Refract. Met. Hard Mater. 83 (2019) 104966. https://doi.org/10.1016/j.ijrmhm.2019.05.012.

[45] M. Richou, A. Durif, M. Lenci, M. Mondon, M. Minissale, L. Gallais, G. Kermouche, G. De Temmerman, Recrystallization at high temperature of two tungsten materials complying with the ITER specifications, J. Nucl. Mater. 542 (2020) 152418. https://doi.org/10.1016/j.jnucmat.2020.152418.

[46] L. Tanure, D. Terentyev, V. Nikolić, J. Riesch, K. Verbeken, EBSD characterization of pure and K-doped tungsten fibers annealed at different temperatures, J. Nucl. Mater. 537 (2020). https://doi.org/10.1016/j.jnucmat.2020.152201.

[47] P. Lied, C. Bonnekoh, W. Pantleon, M. Stricker, A. Hoffmann, J. Reiser, Comparison of K-doped and pure cold-rolled tungsten sheets: As-rolled condition and recrystallization behaviour after isochronal annealing at different temperatures, Int. J. Refract. Met. Hard Mater. 85 (2019) 105047. https://doi.org/10.1016/j.ijrmhm.2019.105047.

[48] A. Alfonso, D. Juul Jensen, G.N. Luo, W. Pantleon, Recrystallization kinetics of warm-rolled tungsten in the temperature range 1150-1350 °c, J. Nucl. Mater. 455 (2014) 591–594. https://doi.org/10.1016/j.jnucmat.2014.08.037.

[49] F.Z. Xia, H.G. Wei, M.P. Wang, D.H. Zhu, Investigation of normal recrystallization and abnormal recrystallization in pure tungsten sheet by EBSD, Int. J. Refract. Met. Hard Mater. 52 (2015) 98–103. https://doi.org/10.1016/j.ijrmhm.2015.05.009.

[50] S. Nogami, A. Hasegawa, M. Fukuda, M. Rieth, J. Reiser, G. Pintsuk, Mechanical properties of tungsten: Recent research on modified tungsten materials in Japan, J. Nucl. Mater. 543 (2021) 152506. https://doi.org/10.1016/j.jnucmat.2020.152506.

[51] K. Wang, X. Zan, M. Yu, W. Pantleon, L. Luo, X. Zhu, P. Li, Y. Wu, Effects of thickness reduction on recrystallization process of warm-rolled pure tungsten plates at 1350 °C, Fusion Eng. Des. 125 (2017) 521–525. https://doi.org/10.1016/j.fusengdes.2017.03.140.

[52] K. Wang, D. Ren, X. Zan, L. Luo, X. Zhu, Y. Wu, Recrystallization behavior of pure tungsten hot-rolled with high accumulated strain during annealing at 1250 °C–1350 °C, Mater. Sci. Eng. A. 806 (2021) 140828. https://doi.org/10.1016/j.msea.2021.140828.

[53] G. Pintsuk, S. Antusch, T. Weingaertner, M. Wirtz, Recrystallization and composition dependent thermal fatigue response of different tungsten grades, Int. J. Refract. Met. Hard Mater. 72 (2018) 97–103. https://doi.org/10.1016/j.ijrmhm.2017.11.039.

[54] L. Tanure, A. Bakaeva, A. Dubinko, D. Terentyev, K. Verbeken, Effect of annealing on microstructure, texture and hardness of ITER-specification tungsten analyzed by EBSD, vickers micro-hardness and nano-indentation techniques, J. Nucl. Mater. 524 (2019) 191–199. https://doi.org/10.1016/j.jnucmat.2019.07.005.

[55] U.M. Ciucani, W. Pantleon, Stagnant recrystallization in warm-rolled tungsten in the temperature range from 1150 °C to 1300 °C, Fusion Eng. Des. 146 (2019) 814–817. https://doi.org/10.1016/j.fusengdes.2019.01.088.

[56] K. Wang, H. Sun, X. Zan, U.M. Ciucani, W. Pantleon, L. Luo, Y. Wu, Evolution of microstructure and texture of moderately warm-rolled pure tungsten during annealing at 1300 °C, J. Nucl. Mater. 540 (2020) 152412. https://doi.org/10.1016/j.jnucmat.2020.152412.

[57] J. Reiser, C. Bonnekoh, T. Karcher, W. Pfleging, D. Weygand, A. Hoffmann, Recrystallisation towards a single texture component in heavily cold rolled tungsten (W) sheets and its impact on micromechanics, Int. J. Refract. Met. Hard Mater. 86 (2020) 105084. https://doi.org/10.1016/j.ijrmhm.2019.105084.

[58] X.-X. Zhang, Q.-Z. Yan, C.-T. Yang, T.-N. Wang, M. Xia, C.-C. Ge, Recrystallization temperature of tungsten with different deformation degrees, Rare Met. 35 (2016) 566–570. https://doi.org/10.1007/s12598-014-0315-2.

[59] U.M. Ciucani, A. Thum, C. Devos, W. Pantleon, Isothermal annealing of thin rolled tungsten plates in the temperature range from 1300 °C to 1400 °C, Nucl. Mater. Energy. 15 (2018) 128–134. https://doi.org/10.1016/j.nme.2018.03.009.

[60] K. Tsuchida, T. Miyazawa, A. Hasegawa, S. Nogami, M. Fukuda, Recrystallization behavior of hot-rolled pure tungsten and its alloy plates during high-temperature annealing, Nucl. Mater. Energy. 15 (2018) 158–163. https://doi.org/10.1016/j.nme.2018.04.004.

[61] S. Krimpalis, K. Mergia, S. Messoloras, A. Dubinko, D. Terentyev, K. Triantou, J.

Reiser, G. Pintsuk, Comparative study of the mechanical properties of different tungsten materials for fusion applications, Phys. Scr. T170 (2017) 014068. https://doi.org/10.1088/1402-4896/aa9292.

[62] S. Bonk, J. Reiser, J. Hoffmann, A. Hoffmann, Cold rolled tungsten (W) plates and foils: Evolution of the microstructure, Int. J. Refract. Met. Hard Mater. 60 (2016) 92–98. https://doi.org/10.1016/J.IJRMHM.2016.06.020.

[63] J.C. Sublet, I.P. Bondarenko, G. Bonny, J.L. Conlin, M.R. Gilbert, L.R. Greenwood, P.J. Griffin, P. Helgesson, Y. Iwamoto, V.A. Khryachkov, T.A. Khromyleva, A.Y. Konobeyev, N. Lazarev, L. Luneville, F. Mota, C.J. Ortiz, D. Rochman, S.P. Simakov, D. Simeone, H. Sjostrand, D. Terentyev, R. Vila, Neutron-induced damage simulations: Beyond defect production cross-section, displacement per atom and iron-based metrics, Eur. Phys. J. Plus. 134 (2019) 350. https://doi.org/10.1140/epjp/i2019-12758-y.

[64] V. Chatzikos, K. Mergia, G. Bonny, D. Terentyev, D. Papadakis, G.E. Pavlou, S. Messoloras, Positron annihilation spectroscopy investigation of defects in neutron irradiated tungsten materials, Int. J. Refract. Met. Hard Mater. 105 (2022) 105838. https://doi.org/10.1016/j.ijrmhm.2022.105838.

[65] D. Giebel, J. Kansy, LT10 Program for Solving Basic Problems Connected with Defect Detection, Phys. Procedia. 35 (2012) 122–127. https://doi.org/10.1016/j.phpro.2012.06.022.

[66] W.W. Mullins, Theory of Thermal Grooving, J. Appl. Phys. 28 (1957) 333–339. https://doi.org/10.1063/1.1722742.

[67] P. Sachenko, J.H. Schneibel, J.G. Swadener, W. Zhang, Experimental and simulated grain boundary groove profiles in tungsten, Philos. Mag. Lett. 80 (2000) 627–631. https://doi.org/10.1080/09500830050134345.

[68] P. Sachenko, J.H. Schneibel, W. Zhang, Effect of faceting on the thermal grain-boundary grooving of tungsten, Philos. Mag. A Phys. Condens. Matter, Struct. Defects Mech. Prop. 82 (2002) 815–829. https://doi.org/10.1080/01418610208243204.

[69] D. Tarras Madsen, U.M. Ciucani, A. Hoffmann, W. Pantleon, Thermal stability of thin rolled potassium-doped tungsten sheets during annealing at temperatures up to 1400 °C, Nucl. Mater. Energy. 30 (2022) 101126. https://doi.org/10.1016/j.nme.2022.101126.

[70] D. Papadakis, S. Dellis, V. Chatzikos, E. Manios, I.E. Stamatelatos, S. Messoloras, K. Mergia, Neutron irradiation effects in different tungsten microstructures, Phys. Scr. 96 (2021) 124041. https://doi.org/10.1088/1402-4896/ac1eb2.

[71] M. Eldrup, B.N.N. Singh, Studies of defects and defect agglomerates by positron annihilation spectroscopy, J. Nucl. Mater. 251 (1997) 132–138. https://doi.org/10.1016/S0022-3115(97)00221-3.

[72] T. Troev, E. Popov, N. Nankov, T. Yoshiie, Model calculation of positron states in tungsten containing hydrogen and helium, J. Phys. Conf. Ser. 207 (2010) 12033. https://doi.org/10.1088/1742-6596/207/1/012033.

[73] A.D. Brailsford, R. Bullough, The rate theory of swelling due to void growth in irradiated metals, J. Nucl. Mater. 44 (1972) 121–135. https://doi.org/10.1016/0022-3115(72)90091-8.

[74] M. Klimenkov, M. Dürrschnabel, U. Jäntsch, P. Lied, M. Rieth, H.C. Schneider, D. Terentyev, W. Van Renterghem, Microstructural analysis of W irradiated at different

temperatures, J. Nucl. Mater. 572 (2022) 154018. https://doi.org/10.1016/j.jnucmat.2022.154018.

[75] M. Dürrschnabel, M. Klimenkov, U. Jäntsch, M. Rieth, H.C. Schneider, D. Terentyev, New insights into microstructure of neutron-irradiated tungsten, Sci. Rep. 11 (2021) 1–17. https://doi.org/10.1038/s41598-021-86746-6.

[76] G. Bonny, M.J. Konstantinovic, A. Bakaeva, C. Yin, N. Castin, K. Mergia, V. Chatzikos, S. Dellis, T. Khvan, A. Bakaev, A. Dubinko, D. Terentyev, Trends in vacancy distribution and hardness of high temperature neutron irradiated single crystal tungsten, Acta Mater. 198 (2020) 1–9. https://doi.org/10.1016/j.actamat.2020.07.047.

[77] W. Brandt, R. Paulin, Positron diffusion in solids, Phys. Rev. B. 5 (1972) 2430–2435. https://doi.org/10.1103/PhysRevB.5.2430.

[78] W. Pantleon, Thermal stability of the microstructure in rolled tungsten for fusion reactors, Phys. Scr. 96 (2021) 124036. https://doi.org/10.1088/1402-4896/ac2854.

[79] A. Alfonso, D. Juul Jensen, G.N. Luo, W. Pantleon, Thermal stability of a highly-deformed warm-rolled tungsten plate in the temperature range 1100-1250 °c, Fusion Eng. Des. 98–99 (2015) 1924–1928. https://doi.org/10.1016/j.fusengdes.2015.05.043.

[80] U.M. Ciucani, A. Thum, C. Devos, W. Pantleon, Recovery and recrystallization kinetics of differently rolled, thin tungsten plates in the temperature range from 1325 °C to 1400 °C, Nucl. Mater. Energy. 20 (2019) 100701. https://doi.org/10.1016/j.nme.2019.100701.

[81] M. Yu, K. Wang, X. Zan, W. Pantleon, L. Luo, X. Zhu, Y. Wu, Hardness loss and microstructure evolution of 90% hot-rolled pure tungsten at 1200–1350 °C, Fusion Eng. Des. 125 (2017) 531–536. https://doi.org/10.1016/j.fusengdes.2017.05.072.

[82] A. Godfrey, D. Juul Jensen, N. Hansen, Recrystallisation of channel die deformed single crystals of typical rolling orientations, Acta Mater. 49 (2001) 2429–2440. https://doi.org/10.1016/S1359-6454(01)00148-3.

[83] P. Schade, 100years of doped tungsten wire, Int. J. Refract. Met. Hard Mater. 28 (2010) 648–660. https://doi.org/10.1016/j.ijrmhm.2010.05.003.

[84] P. Schade, H.M. Ortner, I. Smid, Refractory metals revolutionizing the lighting technology: A historical review, Int. J. Refract. Met. Hard Mater. 50 (2015) 23–30. https://doi.org/10.1016/j.ijrmhm.2014.11.002.

[85] M.A.T. Thompson, K. Song, G. De Temmerman, H. Chen, N. Kirby, J. Bradby, D. Bhattacharyya, C. Hoang, C.S. Corr, Identifying microstructural changes responsible for retarded grain growth during tungsten recrystallization after helium plasma exposure, J. Nucl. Mater. 559 (2022) 153448. https://doi.org/10.1016/j.jnucmat.2021.153448.

[86] W. Guo, S. Wang, K. Xu, Y. Zhu, X.-X. Wang, L. Cheng, Y. Yuan, E. Fu, L. Guo, G. De Temmerman, G.-H. Lu, Effect of helium ion irradiation on tungsten recrystallization, Phys. Scr. T171 (2020) 014004. https://doi.org/10.1088/1402-4896/ab36d8.

[87] W. Guo, L. Cheng, G. De Temmerman, Y. Yuan, G.-H. Lu, Retarded recrystallization of helium-exposed tungsten, Nucl. Fusion. 58 (2018) 106011. https://doi.org/10.1088/1741-4326/aad2b0.

[88] K. Song, M. Thompson, G. De Temmerman, C.S. Corr, Temperature dependence of retarded recrystallisation in helium plasma-exposed tungsten, Nucl. Fusion. 59 (2019). https://doi.org/10.1088/1741-4326/ab2e3c.

[89] A. Hasegawa, T. Miyazawa, D. Itou, T. Hattori, K. Yohida, S. Nogami, Helium effects on recovery and recrystallization of powder metallurgically processed tungsten, Phys. Scr. T171 (2020) 014016. https://doi.org/10.1088/1402-4896/ab408d.

[90] T. Wang, X. Wang, X. Ma, L. Cheng, Y. Yuan, W. Guo, K. Xu, M. Liu, Z. Xie, L. Guo, G.-H. Lu, Neon-concentration dependent retarding effect on the recrystallization of irradiated tungsten: Experimental analysis and molecular dynamics simulation, J. Mater. Sci. Technol. 139 (2023) 245–259. https://doi.org/10.1016/j.jmst.2022.09.031.

[91] V. Shah, J.T.S. Beune, Y. Li, T. Loewenhoff, M. Wirtz, T.W. Morgan, J.A.W. van Dommelen, Recrystallization behaviour of high-flux hydrogen plasma exposed tungsten, J. Nucl. Mater. 545 (2021) 152748. https://doi.org/10.1016/j.jnucmat.2020.152748.